5-21-2013

Direct pulsed laser crystallization of nanocrystals for absorbent layers in photovoltaics: Multiphysics simulation and experiment

Martin Y. Zhang
Purdue University

Qiong Nian
Purdue University, qnian@purdue.edu

Yung Shin
Purdue University, shin@purdue.edu

Gary J. Cheng
Birck Nanotechnology Center, Purdue University, gjcheng@purdue.edu

Zhang, Martin Y.; Nian, Qiong; Shin, Yung; and Cheng, Gary J., "Direct pulsed laser crystallization of nanocrystals for absorbent layers in photovoltaics: Multiphysics simulation and experiment" (2013). *Birck and NCN Publications.* Paper 1399.
http://dx.doi.org/10.1063/1.4805039

AIP | Journal of Applied Physics

Direct pulsed laser crystallization of nanocrystals for absorbent layers in photovoltaics: Multiphysics simulation and experiment

Martin Y. Zhang, Qiong Nian, Yung Shin, and Gary J. Cheng

Citation: J. Appl. Phys. **113**, 193506 (2013); doi: 10.1063/1.4805039
View online: http://dx.doi.org/10.1063/1.4805039
View Table of Contents: http://jap.aip.org/resource/1/JAPIAU/v113/i19
Published by the AIP Publishing LLC.

Direct pulsed laser crystallization of nanocrystals for absorbent layers in photovoltaics: Multiphysics simulation and experiment

Martin Y. Zhang,[1] Qiong Nian,[1] Yung Shin,[2] and Gary J. Cheng[1,2,3,a)]
[1]*School of Industrial Engineering, Purdue University, West Lafayette, Indiana 47906*
[2]*School of Mechanical Engineering, Purdue University, West Lafayette, Indiana 47906*
[3]*Birck Nanotechnology Center, Purdue University, West Lafayette, Indiana 47906*

(Received 2 April 2013; accepted 29 April 2013; published online 17 May 2013)

Direct pulsed laser crystallization (DPLC) of nanoparticles of photoactive material—Copper Indium Selenide (nanoCIS) is investigated by multiphysics simulation and experiments. Laser interaction with nanoparticles is fundamentally different from their bulk counterparts. A multiphysics electromagnetic-heat transfer model is built to simulate DPLC of nanoparticles. It is found smaller photoactive nanomaterials (e.g., nanoCIS) require less laser fluence to accomplish the DPLC due to their stronger interactions with incident laser and lower melting point. The simulated optimal laser fluence is validated by experiments observation of ideal microstructure. Selectivity of DPLC process is also confirmed by multiphysics simulation and experiments. The combination effects of pulse numbers and laser intensity to trigger laser ablation are investigated in order to avoid undesired results during multiple laser processing. The number of pulse numbers is inversely proportional to the laser fluence to trigger laser ablation. © *2013 AIP Publishing LLC*.
[http://dx.doi.org/10.1063/1.4805039]

I. INTRODUCTION

Nanoparticles, those particles with diameter ranging from a few nanometers to several hundreds of nanometers, are of great interest in nanotechnology and nanoscience today. Due to small sizes, properties of nanoparticles differ significantly from bulk counterparts for example, low melting temperature for nanoparticles so as to realize low temperature processing.[1] Prior research also found that higher plasmon resonances induced stronger interactions between laser and nanoparticles.[2]

A schematic of heat energy exchange between laser and nanoparticles is illustrated in Figure 1. The interaction between laser and layer of packed nanoparticles will result in resistive heating which can be regarded as secondary heat source (Q_{RH}). Q_{RH} which mainly resides in nanoparticles will cause crystallization, recrystallization, or melting of nanoparticles depending on resulting temperature field in nanoparticles. Such laser-nanoparticles interactions are complicated since laser wavelength is greater than the dimension of nanoparticles, and layer-packed Nanoparticles could not be assumed as continuous materials. An appropriate approach to fully understand the mechanism of this process is to use multiphysics simulation that consists of electromagnetic (EM) and heat transfer (HT) modules.

However, prior understanding of the intrinsic properties of involved nanomaterials is required. Unlike bulk materials, properties of nanoparticles are strongly dependent on particle sizes because of quantum-size effect,[1,3] Coulomb-charging effect,[4] high surface-total atom ratio,[5] high surface area-to-volume ratio,[6] and large surface energy (surface tension).[7] Critical properties, such as electrical and thermal conductivities and heat capacity of nanoparticles will be discussed. electromagnetic-heat transfer (EM-HT) model will be established to describe the DPLC process. Calculated resistive heating and temperature fields for different particle sizes will be discussed. The effects of laser intensities will be studied by both simulation and experiments. The simulation results will be compared with experimental observation to decide optimal processing conditions. The effects of pulse numbers and laser fluence will be investigated.

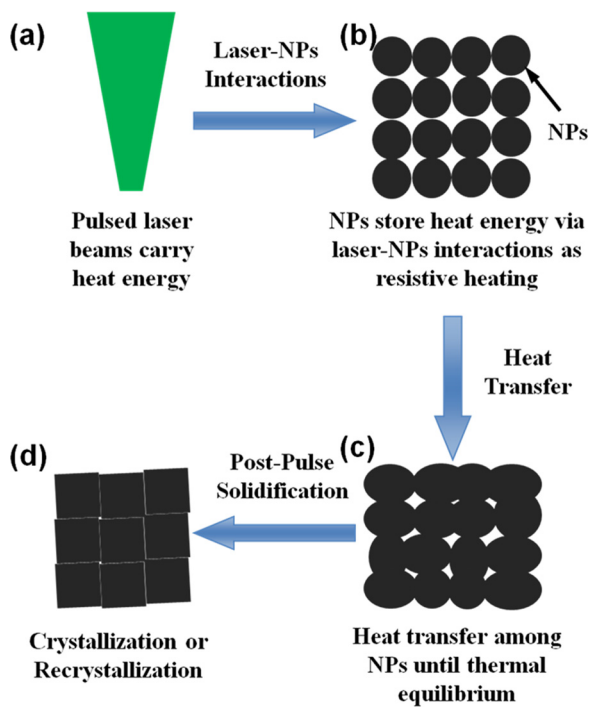

FIG. 1. Schematic of heat energy transportation in laser-nanoparticles interaction process is shown. In the post-pulse solidification stage, the nanoparticles will experience a crystallization or recrystallization process depending on the resulting temperature in previous stages.

[a)]Author to whom correspondence should be addressed. Electronic mail: gjcheng@purdue.edu.

II. SIZE DEPENDENCE OF NANOPARTICLES

In bulk materials, atoms are evenly distributed in the body. The forces on every atom have a good balance which leads to stable physical properties regardless of their sizes. In nanoparticles, however, the cohesive forces at body atoms, refer to b, are balanced among all neighboring atoms. But surface atoms do not have atoms on all sides which results in unbalanced forces; this causes unstable size-dependent properties[8] of nanosized particles.

The second major characteristic of nanoparticles is the surface-to-total atom ratio (N). When particles are of nanometer scale, the ratio of the number of surface atoms to the number of total atoms becomes large[8,9]

$$N = \frac{n_f}{n_t}, \tag{1}$$

where n_f denotes the number of atoms on surface and n_t denotes the number of total atoms. Considering the size is in nanometer scale, the ratio N is much higher than that of bulk materials. Other than N, nanoparticles also have a larger surface-area-to-volume ratio,[6] assuming nanoparticles are spheres

$$r_{sv} = \frac{S}{V} = \frac{4\pi r^2}{\frac{4\pi r^3}{3}} = \frac{3}{r}, \tag{2}$$

where r denotes the radius of particles. From Eq. (2), for a nanoparticle with d of 30 nm, for instance, the r_{sv} is in the order of 108 (m^{-1}), and it increases with decreasing of d.

Size dependent of nanoparticles on melting point (T_m), thermal and electrical conductivities (κ, σ), and specific heat capacity (C_p) is considered.

A. Size dependence on melting point (T_m)

The size dependent of melting point of small particles ($T_{m,p}$) was first studied by Takagi,[10] Blackman and Curzon,[11] and Wronski.[12] It is found that reduction of melting temperature of nanoparticles is expected, and it is size-dependent, with some certain correlation between $T_{m,p}$ and $1/d$. A well-accepted correlation between melting temperature and inverse of particle sizes is stated in Eq. (3a) for very small nanoparticles (i.e., <10 nm)[8,9,13,14]

$$T_{m,p} = T_{m,b} \cdot \left(1 - \frac{a}{bd + 2a/3 - 5b/3}\right), \tag{3a}$$

where $T_{m,p}$ and $T_{m,b}$ are the melting point of nanoparticle and bulk, respectively. Factors $a = 2P_S d$, $b = P_L$ are material-dependent. For large nanoparticles (i.e., >80 nm), the melting point should follow[8]

$$T_{m,p} = T_{m,b} \cdot \left(1 - \frac{4P_S R}{P_L d}\right), \tag{3b}$$

where R is the atomic radius of the corresponding element. Equations (3) are used to calculate for the melting point of nanoparticles ranging from 3 nm to 800 nm.

B. Size dependence on conductivities (κ, σ)

Thermal conductivity (κ) is a measure of the ease with which heat energy can be transferred through a material. Bidwell[15,16] and Wilson[17] combined classical physics with modern physics and gave a universal definition of κ of bulk material

$$\kappa = \frac{1}{3}\rho C_p \lambda_T v_m + \frac{\pi^2 n k_B^2 T \tau}{3m}. \tag{4}$$

Equation (4) can be used to calculate for κ when C_p of the same substance is known. According to Eq. (4), κ is a constant to a substance. However, thermal conductivity of a nanoscale substance is found to be greatly differing from bulk, where Eq. (4) does not hold.

Various studies have been carried out to study the size dependent thermal conductivity.[18–21] By applying Matthiessen's rule[19,21] which considers thermal resistivity (equals to $1/\kappa$) of nanoparticles as the sum of the resistivity of bulk materials (lattice vibration's contribution) and resistivity due to particle size (boundary's contribution), a rough approximation of thermal conductivities of nanoCIS could be obtained. In current EM-HT module, conductivities of larger particles (from 200 to 600 nm) are the same as bulk counterparts, conductivities of medium nanoparticles (from 10 to 80 nm) are one order of magnitude less than bulk counterparts, and for very small nanoparticles (<10 nm) conductivities are about two orders of magnitude less than their bulk counterparts.

Electrical conductivity measures the ability of a material to conduct an electric current, which is how easily electrons are able to flow through a material. From solid-state physics, thermal and electrical conductions are intrinsically correlated and determined by the ability of electrons to move in the substance. Wiedemann-Franz-Lorenz law[22–24] depicts the correlation between electrical conductivity (σ) and thermal conductivity (κ) of the same substance

$$\frac{\kappa}{\sigma} = LT, \tag{5}$$

where the coefficient L is called Lorenz number. Equation (5) describes the correlation between σ and κ universally. Therefore, for nanoparticles with known thermal conductivity, their σ could be obtained from Eq. (5) accordingly.

C. Size dependence on specific heat capacity (C_p)

Heat capacity (C) is defined by the temperature (T) derivative of the internal energy (U). In 1912, Debye gave the T^3 law of specific heat that large scale substance.[25] However, Debye's T^3 law is not valid for substance in the nanometer scale. Shrivastava[26] found that due to boundary scattering effect, the correlation between C and T should include an exponential component based on Debye's T^3 law

$$C_p = \frac{\partial E(T)}{\partial T} \cong 4b_1 T^3 \exp(-b_0 T), \tag{6}$$

where $b_0 = k_B d/(\hbar\pi\nu)$. Equation (6) describes a modification of the Debye's T^3 law for nanocrystals. Higher C_p of

TABLE I The size effects of nanoCIS on melting point (Tm), conductivities (κ, σ), and heat capacity (Cp) at different sizes used in this study.[30–32]

CIS	Bulk	600 nm	300 nm	150 nm	50 nm	25 nm
T_m (K)	1259	1255	1252	1249	1212	1167
κ (W/m K)	8.6	8.6	8.6	8.6	4	0.86
σ (S/m)	1×10^{-4}	1×10^{-4}	1×10^{-4}	5×10^{-5}	2×10^{-5}	1×10^{-5}
C_p (J/kg K)	99	99	95	90	80	70

nanoparticles than bulk polycrystalline have been found for Pd (50% higher), Cu (10% higher), and Pd (40% higher).[27] Considering size effects, modified specific heat of nanocrystals can be written as

$$C_p \cong 4b_1T^3\exp[-k_BTd/(\hbar\pi\nu)] = c_1\exp(-\alpha d), \quad (7)$$

where $\alpha = k_BT/(\hbar\pi\nu)$, and $c_1 = 4b_1T^3$. Equation (7) could be used to determine C_p for nanosized particles at a given T. It is obvious that there is a large change in C_p for a small change in d of the nanoparticles.

In multiphysics EM-HT simulation used in current article, all involved parameters of are based on calculated size dependent properties. The size effects of nanoCIS on melting point, thermal and electrical conductivities, specific heat capacity were listed in Table I.

III. SIMULATION METHODS

A. Multiphysics EM-HT model

In order to understand the mechanism of DPLC process and select appropriate processing parameters, a finite element analysis (FEA) model is built at the COMSOL MULTIPHYSICS software platform. The Schematic of multiphysics simulation model is shown in Figure 2. This model uses an EM module to simulate the laser-nanoparticle interaction, and a HT module to simulate the heat conduction as a result of laser heating. Resistive heating (Q_{RH}), the output from EM module is coupled to HT module as the secondary heat source which eventually causes temperature elevation. The physical properties, such as electrical and thermal conductivity, heat capacity of involved nanomaterials are also important to this model. Considering the size effects, calculated size dependent properties of nanomaterials were used. When laser source, initial conditions and boundary conditions are carefully selected, the EM-HT model could be properly built and solved.

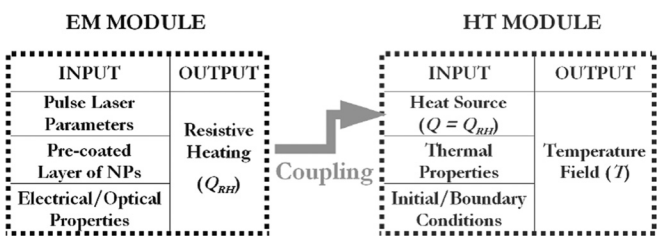

FIG. 2. Schematic of EM-HT simulation model. EM module was solved to obtain resistive heating in step 1. In step 2, the coupled HT model with resistive heating as heat source was solved to acquire the final temperature distribution.

Laser beams are assumed to be in the fundamental (TEM_{00}) mode with wavelength of 532 and 248 nm for DPLC. Primary controlling parameters to laser are laser pulse energy (E), pulse duration (τ), and beam radius (r). The spatial distribution of laser pulse can be written as

$$E = E_o \cdot \exp\left[-2\left(\frac{x^2}{r^2} + \frac{y^2}{r^2}\right)\right], \quad (8)$$

where E_o denotes the central pulsed energy of laser beam, and x, y are the axes for the 2D coordinate. Temporal distribution of the laser is represented using normalized Weibull function which could manipulate the pulse duration and power by modifying its shape factors.

B. Resistive heating (Q_{RH}) and temperature (T)

The pre-deposited layer is composed of tightly packed photoactive and/or TCO nanoparticles. Incident laser beam would be scattered by those nanoparticles; as a result, near-field scattering occurs which enhances the local intensity on the pre-deposited layer surface. The accumulation of enhanced intensities then releases in the form of resistive heating (Q_{RH}), which could be expressed as follows:[28]

$$Q_{RH} = \frac{1}{2}\mathrm{Re}\{\sigma EE^* - j\omega ED^*\}. \quad (9)$$

The governing equations in the EM module are Ampère's law with Maxwell's correction and Faraday's law of induction. These equations depict the time and space of EM field in free space. Due to the conservation of energy for the electromagnetic field

$$\int_V J \cdot EdV + \oint_V (E \times H) \cdot nds = -\int_V \left(E\frac{\partial D}{\partial t} + H\frac{\partial B}{\partial t}\right)dV, \quad (10)$$

where on the left-hand-side, the first term represents the resistive losses, and the second term represents the radiative losses. Equations (9) and (10) are then numerically solved in EM module when laser parameters, materials properties of nanoparticles, and pre-coated layer properties are input into the model.

As heat transfer occurs, temperature (T) would form in the system. A typical T field is given by solving a coupled HT module with prior calculated Q_{RH} inputting as the heat source. The HT module renders the fact that heat energy exchanged among laser, nanoparticles and substrate in the system (Figure 1). The rate of heat conductions strongly depend on nanomaterials themselves, including thermal conductivity, specific heat capacity and density. Directly heated up by laser beam (stage 1), target nanoparticles accumulate heat energy which might cause surface melting (stage 2) assuming melting point is reached and in the following 20 ps[29] or so, surface melting starts to occur. EM-HT simulation reveals that for a pulse laser irradiation (pulse width: 25 ns), it will take ~54 ns to reach melting temperature, which is a few ns later than the peak of resistive heating. After peak point, temperature starts to drop. After certain

period of time, temperature eventually drops to room temperature (300 K). During this time period, heat energy stored in nanoparticles is transferred among neighboring nanoparticles until thermal equilibrium arrives (stage 3).

C. Simulation of DPLC of photoactive nanoparticles

The model is set up consisting of CIS/Mo/SLG layers: the substrate is a standard 500 nm molybdenum (Mo) sputtered soda lime glass (SLG) with rolling-printing of 2 μm thick CIS photoactive materials on top. A typical CIS/Mo/SLG structure before laser crystallization is shown in Figure 3(b). In this configuration, SLG is highly transparent to visible and near infrared light (e.g., 532 nm and 1064 nm), Mo is highly reflective, thus absorption is very limited throughout the laser wavelength under investigation. Therefore, in this case, both 532 nm and 1064 nm have been tried with DPLC to process the samples. Considering the band gap of CIS is ~1.04 eV; therefore, both 532 and 1064 nm are suitable for processing CIS.

In constructing the multiphysics 2D model (Figure 3(a)), it is assumed that CIS nanoparticles are perfect spheres of uniform size and in close contact. The effects of non-uniformity in particle size and distribution on temperature distribution are not considered in this model and will be considered in the future studies. A 2-μm-thick photoactive layer, consisted of a large number of CIS nanoparticles, is employed in this case. Sputtered Mo layer is regarded as square pillars with width (equals to diameter of columns from the 3D point of view) ranging from 10 to 30 nm (see Figure 3(b)) and length of 500 nm (thickness of Mo layer). SLG is used as the supporting substrate with relatively infinity length compared with that of CIS and Mo layers. In reality, in order to rationalize the computation time, the model size is limited to 20 × 40 μm in size.

In this multiphysics model, the most important parameters are applied laser parameters including laser wavelength (λ: nm), laser pulse energy (E: mJ), laser beam radius (r: mm) and laser scan speed (v: mm/s). In the electromagnetic (EM) module, electrical conductivity, refractive index, and material transparency (relative to applied laser wavelength) of involved materials are key inputs; in the heat transfer (HT) module, thermal conductivity, specific heat capacity and density of involved materials are key inputs. All material properties are size dependent as discussed earlier in this article and are listed in Table I for reference. After selecting appropriate boundary and initial conditions, the EM-HT multiphysics model could be computed at the COMSOL software platform. One of the key outputs of EM module is resistive heating (Q_{RH}) and it is treated as the input heat source to the coupled HT module with key output of interest to be the resulting temperature (T), as shown in Figure 3(c).

In the parametric analysis, the resulting T is strongly related to input materials properties such as nanoparticle size (d: nm), laser parameters such as E and r, or simply stated as the laser fluence (F: mJ/cm^2). Similar model with different

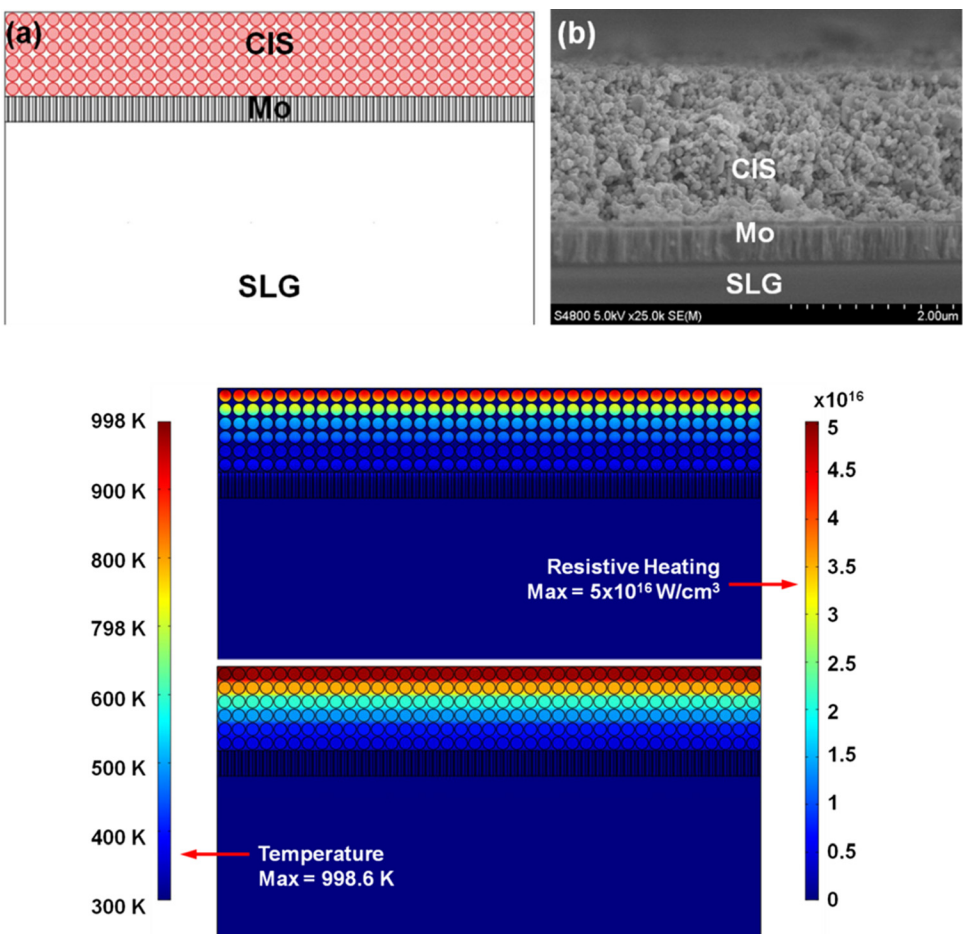

FIG. 3. (a) Multiphysics modeling setup of multilayers in DPLC of CIS; (b) Actual cross sectional view of CIS/Mo/SLG FESEM image; (c) Representative resistive heating (QRH) and temperature (T) fields as a result of DPLC processing of CIS nanoparticles (50 nm) with laser fluence of 24 mJ/cm^2 after one pulse.

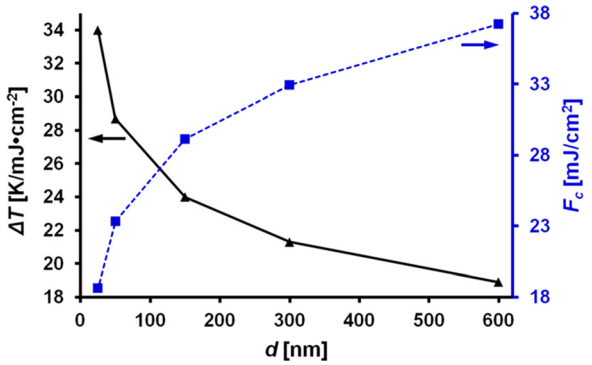

FIG. 4. CIS nanoparticle size dependence on temperature raise per unit laser fluence (ΔT, solid curve with triangle symbols) and laser fluence needed to reach crystallization (F_c, dashed curve with square symbols) as a result of DPLC.

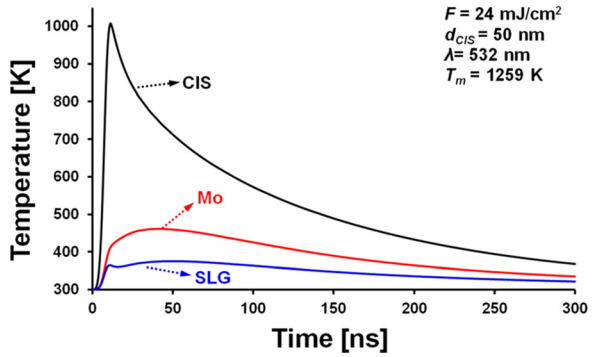

FIG. 5. Temperature distribution in different layers of a CIS/Mo/SLG configuration as a result of DPLC processing.

nanoparticle size d is built to investigate the dependence of d on resulting T as a result of different input laser fluence (F). In order to trigger crystallization processes, the resulting temperature is aimed to the melting point of nanoparticles ($T_{m,p}$), which is size dependent and less than that of the bulk ($T_{m,b}$).

It is found that the temperature raise per unit laser fluence (ΔT: K/mJ·cm^{-2}) is strongly dependent on the size of nanoparticles and the smaller the nanoparticles are, the larger then ΔT is as shown in (Figure 4). For nanoCIS with diameter of 25, 50, 150, 300, and 600 nm, the corresponding ΔT is 34.1, 28.7, 24, 21.3, and 18.9 K/mJ·cm^{-2}, respectively. The nanoscale size effect on laser-nanoparticles interactions is responsible for this effect since smaller nanoparticles have stronger interactions with laser[32,33] thus resulting in larger resistive heating and temperature elevation.

Considering smaller nanoparticles have lower melting point than larger counterparts, it is clear that DPLC of smaller nanoparticles usually requires less laser fluence and the processing temperature is usually lower. The required laser fluence to trigger crystallization nanoparticles (F_c: ~80% of corresponding melting point) is also plotted against nanoparticles size (d). As depicted in dashed curve with square symbols in Figure 4, the laser fluence used to crystallize CIS nanoparticles with diameter of 25, 50, 150, 300, and 600 nm is 18.6, 23.3, 29.1, 32.9, and 37.2 mJ/cm^2, respectively. Therefore, by using smaller nanoparticles, lower temperature processing with smaller laser energy used is possible for DPLC processes. This agrees with what we have found in experiments (other submitted but not published manuscript). In our recent series of experiments, we have found that laser fluence of 24mJ/cm^2 is enough to end up with crystallization of CIS nanoparticles (mixture of CIS nanoparticles with diameters ranging from 10 to 50 nm).

The investigation to the temperature profiles in other layers of the CIS/Mo/SLG configuration found that even if temperature of CIS layer is as high as ~1000 K, the peak temperatures in the Mo and SLG layers are 470 and 385 K, respectively (Figure 5). These are fairly low temperatures for Mo and SLG compared with RTA process where the entire unit is placed in a furnace to experience 400–450 C temperature for a certain period of time. DPLC would effectively protect Mo and SLG layers from overheating and potentially DPLC would be employed to process thin film solar cells or other electronic devices on low melting point substrate such as polymer and regular printing papers.

IV. EXPERIMENTAL METHODS AND MODELING VALIDATION

Continuum Surelite^{TM} series Nd:YAG pulsed laser operated at second harmonic generation (SHG, 535 nm) is used. The laser pulse duration is 5 ns. Different laser fluencies could be applied by adjusting the power attenuator and beam expander to obtain different laser pulse energies and beam sizes. Various laser fluencies and pulse numbers are applied during the experiments.

A. Effects of laser fluence: Modeling and experimental validation

Optimal processing conditions for DPLC of CIS nanocrystals ($d = 20 \sim 40$ nm) were found after series of experiments. Two processing parameters play important roles in DPLC: laser fluence (F), and pulse number (N). When the N was fixed at 30, laser pulses with different F irradiated at the CIS thin film led to completely different surface morphology which was characterized by FESEM and shown in Figure 6. When laser fluence was relatively low (10 mJ/cm^2), very few crystals grow occurred, Figure 6(a). This is because resulting heat energy is inadequate to cause either crystal growth or crystal melting. When laser pulse with a higher F (16 mJ/cm^2) was applied, obvious growth happened to most of crystals but not 100% of them, as shown in Figure 6(b). When 24 mJ/cm^2 is used, crystal growth happens to all crystals resulting in good homogeneity and surface roughness (see Figure 6(c)). Nanoparticles did not exist anymore. Instead, CIS crystals with size in the scale of microns dominated. This clearly shows the growth of CIS crystals and the reduction on internal defects (i.e., inter-crystal gaps, grain boundaries). When laser fluence higher than 24 mJ/cm^2 is used (for example, 34 mJ/cm^2), the film would end up with either poor porous and ablated CIS at the surface Fig. 6(d). These indicate that the ideal laser fluence for CIS material is around 24 mJ/cm^2.

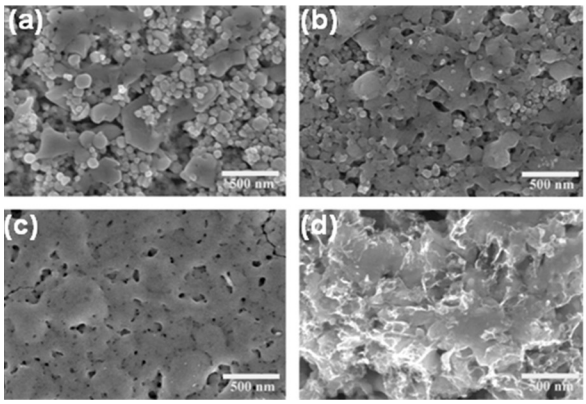

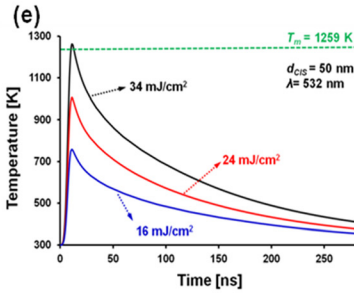

FIG. 6. Morphology characterization of top surface of thin film after DPLC of nanoCIS of various laser fluence: (a) 10 mJ/cm^2: under optimal; (b)16 mJ/cm^2: under optimal; (c) 24 mJ/cm^2: optimal; (d) 34 mJ/cm^2: over optimal; and simulated temperature history of various laser fluences (16, 24, 34 mJ/cm^2)

B. Combinational effects of pulse numbers and laser fluence

It is important to maintain the laser fluence and pulse number at appropriate level in DPLC. If the applied laser fluence is too high, laser ablation might occur to CIS nanocrystals, resulting in decomposition of the CIS layer. On the other hand, a laser with too low fluence is not sufficient to generate crystal growth no matter how many laser pulses are applied. Instead, only smoothening effect was found, while growth of CIS crystals could barely be observed; this is because the heat energy provided is inadequate to overcome the surface energy difference between neighboring boundaries. Meanwhile, the temperature raise within CIS crystals is too low to reach its melting point.

Optimal processing conditions for DPLC of CIS nanocrystals ($d = 20 \sim 40$ nm) was found after series of experiments. When the pulse number was equal to 30, laser pulses with different F irradiated at the CIS thin film led to completely different surface morphology which was characterized by FESEM and shown in Figure 7. Experiments revealed that abnormal grain growth dominates the DPLC of CIS nanoparticles. As seen in Figure 7, there are three distinct stages during the crystallization of nanoparticles: *Phase* (1): with the irradiation of first few laser pulses, discrete nanocrystals are densified as the laser induced pressure generated under the confinement media. The transparent confinement also helps to reduce oxidization when it closely covers the target. It is found that phase one usually started when 3–5 laser pulses were applied. *Phase* (2): when 20–25 laser pulses were applied, melting of CIS occurs. It is found that crystal growth inhomogeneously due to the nonuniform temperature distributions in the nanoparticles. Some molten nanoparticles merged instantly to reduce the total surface and strain energy. *Phase* (3): when more than 25 laser pulses are provided, the neighboring small crystals merge to the large crystals to further reduce the total surface and strain energy. After 30 laser pulses, the crystal growth is completed when the average crystal size reaches 4–5 μm. When more than 30 laser pulses were delivered, porous structure started to form at the surface, and some of the grown crystals were broken into small crystals. The formation of porosity is probably due to the ablation of CIS.

If the applied laser fluence is too high, laser ablation might occur to CIS nanocrystals. Under laser fluence of 30 mJ/cm^2 (Figure 8), experiments revealed that it is impossible to obtain a homogeneous crystal growth for all crystals no matter how many laser pulses are applied. When 20 pulses was applied (a), a few nanocrystals would grow bigger; as irradiating more pulses (b)–(d), not only the surface homogeneity became poorer, and grown crystals became porous.

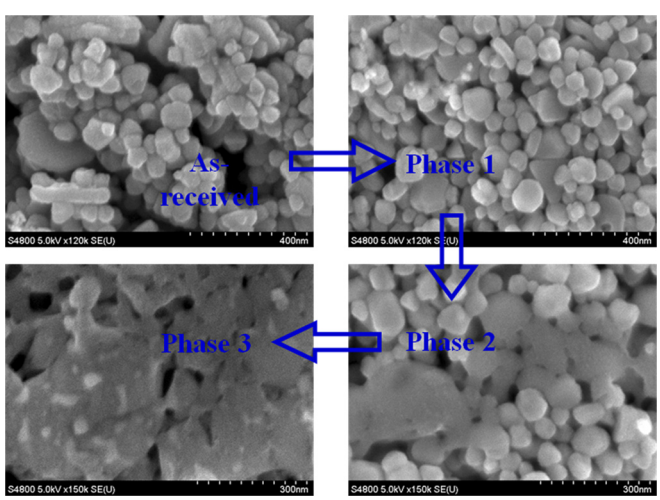

FIG. 7. Mechanism of DPLC of CIS nanocrystal thin film and different phases of crystal growth at 24 mJ/cm^2: (a) as-received, (b) 10 pulses, (c) 20 pulses, and (d) 30 pulses.

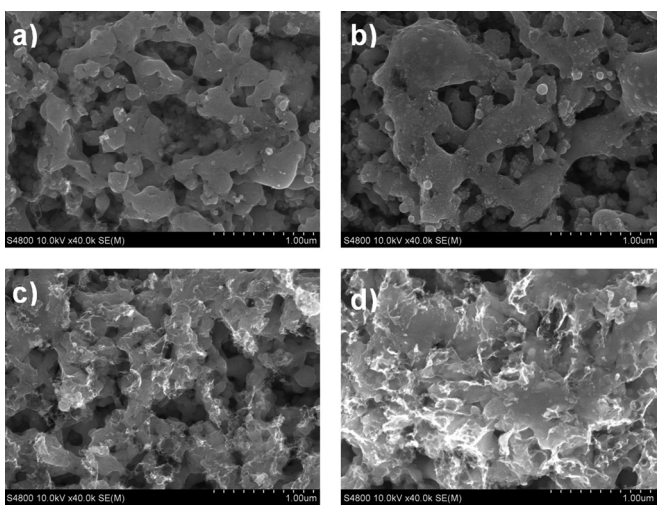

FIG. 8. Top surface morphology of CIS thin film at different pulse number when too high laser was applied (F = 30 mJ/cm^2). (a) 20 pulses, (b) 30 pulses, (c) 35 pulses, and (d) 45 pulses.

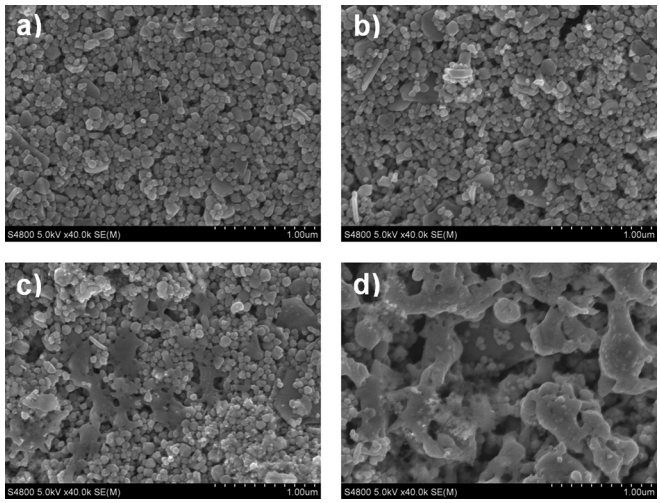

FIG. 9. Top surface morphology of CIS thin film at different pulse number when too low laser was applied (F = 19 mJ/cm^2). (a) 20 pulses, (b) 30 pulses, (c) 35 pulses, and (d) 45 pulses.

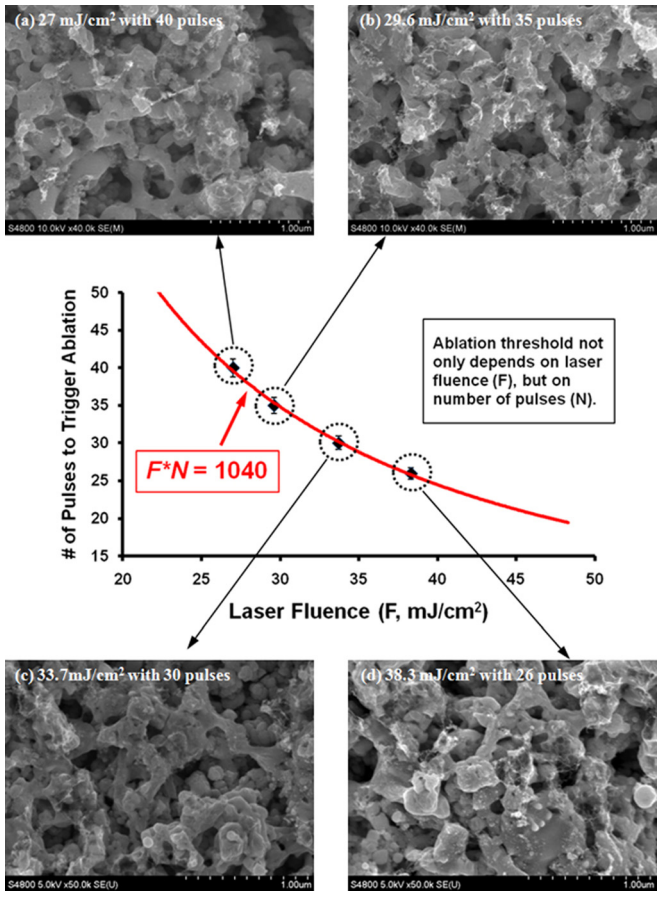

FIG. 10. Combinational effects of laser fluence and pulse number to trigger laser ablation of nanoCIS thin film.

More importantly, obvious ablation starts to occur, which would be likely to have altered the chemical and structural composition of CIS layer.

On the other hand, a laser with too low fluence is not able to produce sufficient crystal growth no matter how many laser pulses are applied. Under laser fluence of 19 mJ/cm^2 (Figures 9(a) and 9(b)), when applying with less than 30 pulses, mainly smoothening effect was found while growth of CIS nanocrystal could barely be observed; this could be explained to be that the heat energy provided is inadequate to overcome the surface energy difference between neighboring boundaries. Meanwhile, the temperature raise within CIS crystals is too low to reach its melting point. Therefore, no crystal growth would occur. When 35 laser pulses are applied, as shown in Figure 9(c), roughly 20% of nanocrystals grew bigger, while the rest were kept unchanged. When 45 pulses were applied, ablation occurred to grown crystals. Therefore, the surface became porous as shown in Figure 9(d).

Ablation of CIS occurs when applied laser exceeds the ablation thresholds. It is found that the ablation threshold of CIS nanocrystals depends not only on laser fluence (F) but on pulse number (N). As mentioned above, there are two situations that might lead to the ablation of CIS: (i) too high laser fluence or (ii) too many laser pulses. Four laser fluence ranging from 27 to 38.3 mJ/cm^2 have been investigated. It is found that for each of the four laser fluence, pulse number to trigger ablation of CIS is different: 40, 35, 30, and 20 pulses for 27, 29.6, 33.7, and 38.3 mJ/cm^2, respectively. If the numbers of pulses to trigger ablation is plotted against corresponding laser fluence, it is found that N is inversely proportional to F when the laser beam area (S) is kept constant. As shown in Figure 10, lower laser fluence needs more pulse number, while higher fluence needs a less pulse number to trigger ablation. This relationship is expected since ablation threshold of the same material is constant, so the totally energy ($F*N*S$) to trigger the ablation should be the same in all cases. This finding could be applied to not only CIS, but other materials. It implies that more effective fabrication process could be employed if lower laser fluence was used so that processing speed (v) could be greatly increased.

V. SUMMARY

In this article, DPLC of CIS nanoparticles are discussed by numerical simulation and experiments. Different from their bulk counterparts, physical properties of nanoparticles such as thermal properties (melting point, heat capacity, and thermal conductivity), and electrical conductivity are size-dependent. A multiphysics EM-HT model is built to simulate DPLC process. During DPLC processing, smaller photoactive nanomaterials (e.g., nanoCIS) have require less laser fluence to accomplish the DPLC due to their stronger interactions with incident laser and lower melting point due to size effect. The simulated optimal laser fluence is validated by experiments observation for ideal microstructure. Selectivity of DPLC process is also confirmed by multiphysics simulation and experiments. Under appropriate laser conditions (including laser wavelength and laser fluence), only the target layer will be heated up, while the rest materials in the system are still at low temperatures. The combinational effects of pulse numbers and laser intensity to trigger laser ablation are investigated in order to avoid undesired results during multiple laser processing. The number of pulse numbers is inverse proportional to the laser fluence to trigger laser ablation.

ACKNOWLEDGMENTS

Financial support from NSF (CMMI 1030786) is appreciated.

[1]M. Schmidt, R. Kusche, B. von Issendorff, and H. Haberland, "Irregular variations in the melting point of size-selected Atomic clusters," Nature (London) **393**, 238–240 (1998).
[2]K. L. Kelly, E. Coronado, L. L. Zhao, and G. C. Schatz, "The optical properties of metal nanoparticles: The influence of size, shape, and dielectric environment," J. Phys. Chem. B **107**, 668–677 (2003).
[3]N. Satoh, T. Nakashima, K. Kamikura, and K. Yamamoto, "Quantum size effect in TiO2 nanoparticles prepared by finely controlled metal assembly on dendrimer templates," Nat. Nanotechnol. **3**, 106–111 (2008).
[4]Y. Volokitin, J. Sinzig, L. J. de Jongh, G. Schmid, M. N. Vargaftik, and I. I. Moiseevi, "Quantum-size effects in the thermodynamic properties of metallic nanoparticles," Nature (London) **384**, 621–623 (1996).
[5]F. Michael, C. Gonzalez, V. Mujica, M. Marquez, and M. A. Ratner, "Size dependence of ferromagnetism in gold nanoparticles: Mean field results," Phys. Rev. B **76**, 224409 (2007).
[6]A. P. Alivisatos, "Perspectives on the physical chemistry of semiconductor nanocrystals," J. Phys. Chem. **100**, 13226–13239 (1996).
[7]K. K. Nanda, A. Maisels, and F. E. Kruis, "Surface tension and sintering of free gold nanoparticles," J. Phys. Chem. C **112**, 13488–13491 (2008).
[8]K. K. Nanda, A. Maisels, F. E. Kruis, H. Fissan, and S. Stappert, "Higher surface energy of free nanoparticles," Phys. Rev. Lett. **91**, 106102 (2003).
[9]A.Safaei, M. A. Shandiz, S. Sanjabi, and Z. Barber, "Modeling the melting temperature of nanoparticles by an analytical approach," J. Phys. Chem. C **112**, 99–105 (2008).
[10]M. Takagi, "Electron-diffraction study of liquid-solid transition of thin metal films," J. Phys. Soc. Jpn. **9**, 359–363 (1954).
[11]M. Blackman and A. E. Curzon, *Structure and Properties of Thin Films* (Wiley, New York, USA, 1953), pp. 217–222.
[12]C. R. M. Wronski, "The size dependence of the melting point of small particles of tin," Br. J. Appl. Phys. **18**, 1731–1737 (1967).
[13]S. J. Zhao, S. Q. Wang, D. Y. Cheng, and H. Q. Ye, "Three distinctive melting mechanisms in isolated nanoparticles," J. Phys. Chem. B **105**, 12857–12860 (2001).
[14]S. L. Lai, J. Y. Guo, V. Petrova, G. Ramanath, and L. H. Allen, "Size-dependent melting properties of small tin particles: Nanocalorimetric measurements," Phys. Rev. Lett. **77**, 99–102 (1996).
[15]C. C. Bidwell, "A simple relation between thermal conductivity, specific heat and absolute temperature," Phys. Rev. **32**, 311–314 (1928).
[16]C. C. Bidwell, "Thermal conductivity of metals," Phys. Rev. **58**, 561 (1940).
[17]A. H. Wilson, *Semi-Conductors and Metals* (Macmillian, New York, USA, 1939).
[18]S. G. Volz and G. Chen, "Molecular dynamics simulation of thermal conductivity of silicon nanowires," Appl. Phys. Lett. **75**, 2056–2058 (1999).
[19]L. Shi, Q. Hao, C. Yu, N. Mingo, X. Kong, and Z. L. Wang, "Thermal conductivities of individual tin dioxide nanobelts," Appl. Phys. Lett. **84**, 2638–2640 (2004).
[20]A. J. Kulkarni and M. Zhou, "Size-dependent thermal conductivity of zinc oxide nanobelts," Appl. Phys. Lett. **88**, 141921 (2006).
[21]J.-K. Yu S. Mitrovic, D. Than, J. Varghese, and J. R. Heath, "Reduction of thermal conductivity in phononic nanomesh structures," Nat. Nanotechnol. **5**, 718–721 (2010).
[22]R. Franz and G. Wiedemann, "Ueber die Wärme-Leitungsfähigkeit der Metalle," Ann. Phys. **165**, 497–531 (1853).
[23]L. Lorenz, "Bestimmung der Wärmegrade in absolutem maasse," Ann. Phys. **223**, 429 (1872).
[24]G. S. Kumar, G. Prasad, and R. O. Pohi, "Review: Experimental determinations of the Lorenz number," J. Mater. Sci. **28**, 4261–4272 (1993).
[25]C. Kittel, *Introduction to Solid State Physics*, 8th ed. (Wiley, NJ, USA, 2005), p. 156.
[26]K. N. Shrivastava, "Specific heat of nanocrystals," Nano Lett. **2**, 21–24 (2002).
[27]L. Gunawan and G. P. Johari, "Specific heat, melting, crystallization, and oxidation of zinc nanoparticles and their transmission electron microscopy studies," J. Phys. Chem. C **112**, 20159–20166 (2008).
[28]COMSOL Multiphysics Manual, Heat Transfer Module, version 3.3.
[29]J. S. Raut, R. B. Bhagat, and K. A. Fichthorn, "Sintering of aluminum nanoparticles: A molecular dynamics study," Nanostruct. Mater. **10**, 837–851 (1998).
[30]A. Rockett and R. W. Birkmire, "$CuInSe_2$ for photovoltaic applications," J. Appl. Phys. **70**(7), R81–R97 (1991).
[31]P. Victora, J. Nagarajub, and S. B. Krupanidhia, "Pulsed excimer laser ablated copper indium diselenide thin films," Solid State Commun. **116**, 649–653 (2000).
[32]M. Y. Zhang and G. J. Cheng, "Nanoscale size dependence on pulsed laser sintering of hydroxyapatite/titanium particles on metal implants," J. Appl. Phys. **108**, 113112 (2010).
[33]P. D. Brewer, J. J. Zinck and G. L. Olsen, "Reversible modification of CdTe surface composition by excimer laser irradiation," Appl. Phys. Lett. **57**, 2526–2528 (1990).